Optical Capillary Fiber Mode Interferometer for Pressure Sensing

Guillermo Salceda-Delgado, Amy Van Newkirk, Jose Enrique Antonio-Lopez, Alejandro Martinez-Rios, Axel Schülzgen, and Rodrigo Amezcua-Correa

***Abstract*—A compact optical fiber pressure sensor is experimentally presented. It consists of a few millimeter long section of a capillary optical fiber spliced between two single-mode fibers (SMFs). Due to the interference between propagating light in the capillary fiber caused by the fundamental core mode of the input SMF, an interference pattern is generated in the transmission spectrum of the device through the output SMF. When pressure is applied to the device, the distributed forces on the capillary tube fiber lead to changes in the visibility of the interference fringes and a wavelength shift. The visibility changes are directly correlated to the pressure applied to the device. The dynamic range of the device can be tailored by selecting a suitable length of the capillary fiber. The response of the device to temperature changes is also discussed.**

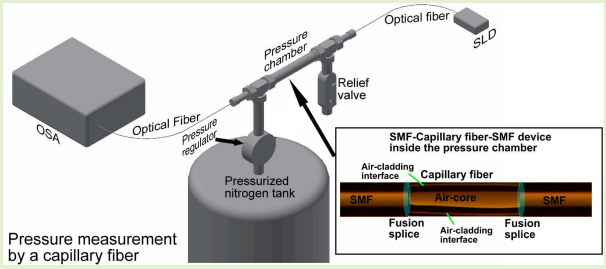

***Index Terms*—Optical interferometry, optical fibers, optical device fabrication, optical sensors, optical fiber devices.**

I. Introduction

OPTICAL fiber sensors have been widely used and are well recognized. The advantages they exhibit for the measurement of physical, chemical, and biomedical parameters are unique. They include immunity to electromagnetic fields, very high sensitivity, long-distance interrogation, small size, fast response, and the capability to operate in extreme or hazardous environments. An important physical parameter to be measured during the operation of industrial systems is pressure, for instance, in pipes, hydropneumatic systems, turbines, etc. [1]. Fiber-optic pressure sensors (FOPSs) have progressed rapidly in the last decades [2]. To date, there are numerous configurations for pressure measurements. Most of these configurations are based on Fabry-Perot resonators (FPRs) [3]. However, the majority of these FPRs are based on the addition of a transducer diaphragm, which deforms when pressure is applied [4]–[11], making the sensor rather complex. Also, FPRs without transducer diaphragm have been reported more recently, but they exhibit complicated and not fully repeatable fabrication process [12] and the need for using a liquid to act as a transducer [13]. On the other hand, several other FOPS configurations, based on fiber Bragg gratings [1], [14], micro-bending of a single-mode fiber (SMF) [15], twin-core fibers [16], [17], and multimode fibers [18] have been proposed. However, some of those methods require an additional transducer, or a complicated fabrication process, resulting in increased costs in sensor complexity. Also, optical fiber pressure sensors with high sensitivity values have been already reported. However, most of them are fabricated with a laborious process, which increases their complexity, cost, operational complexity, and sometimes the sensors become impractical.

Most of the optical fiber sensor configurations use a unique fiber spliced between two SMFs. The particular fiber acts as the sensor head, and the SMFs transmit the information to and from the sensing head. Therefore, the use of novel fibers for sensing applications in a SMF–sensing fiber–SMF structure has become a very useful platform for monitoring a wide variety of physical parameters, such as, temperature, bending and force using multicore fibers [19]–[22], refractive index using a photonic crystal fiber [23], magnetic field using a hollow-core fiber coated with a magnetic gel [24], and strain also with a hollow core fiber [25], to mention just a few.

In this work, we utilize a hollow-core fiber, known as capillary optical fiber (COF) [26], to construct an SMF-COF-SMF structure and form a practical, new, simple, compact, cost-

Manuscript received September 16, 2019; revised November 7, 2019; accepted November 7, 2019. Date of publication November 14, 2019; date of current version February 5, 2020. The associate editor coordinating the review of this article and approving it for publication was Dr. EH Yang. *(Corresponding author: Guillermo Salceda-Delgado.)*

G. Salceda-Delgado is with the Facultad de Ciencias Físico Matemáticas, Universidad Autónoma de Nuevo León, San Nicolás de los Garza, 66455, México (e-mail: guillermo.salcedadl@uanl.edu.mx).

A. V. Newkirk, J. E. Antonio-Lopez, A. Schülzgen, and R. Amezcua-Correa are with CREOL, The College of Optics and Photonics, University of Central Florida, Orlando, FL 32816-2700 USA.

A. Martinez-Rios is with the Centro de Investigaciones en Optica A. C., Lomas del campestre 37150, Mexico.

Digital Object Identifier 10.1109/JSEN.2019.2953683

effective, and attractive interferometric device to be applied as a pressure sensor. The proposed device acts as the transducer by itself, and its fabrication process is carried out just by the use of a splicing machine to splice SMF to COF, and no additional fabrication process is needed.

To build the device, we manufactured a silica capillary fiber with 130 μm and 80 μm of outer and inner diameter, respectively. A few millimeters long segment of this fiber is spliced between two SMFs. Similar devices act as FPRs, and previous analytical and numerical studies have been reported to explain the light propagation behavior caused by the partial reflecting faces of the fibers [27]–[30]. However, according to our SMF-COF-SMF structure and its response, the proposed device here acts as a Mach-Zehnder fiber interferometer (MZFI). The propagated light through the device is the result of the interference caused by the superposition of light guided in the air-core and air-cladding interface of the COF.

Due to refractive index changes because capillary wall deformations when pressure forces are applied to the SMF-COF-SMF structure, accordingly with the photo-elastic effect, the light behavior through the structure allows sensitivity to pressure [31]. The device was placed inside a high-pressure chamber, which was pressurized using nitrogen. A relief valve was used to vary the pressure in a controlled way. With this approach, we were able to measure pressure values ranging from 200 to 1000 psi. Subsequently, additional tests under varying temperature conditions were carried out to examine the behavior of the pressure sensor under the influence of such a perturbation and investigate its effects with the pressure measurement performance.

II. Capillary Fiber Pressure Sensor and Experimental Setup

The fabrication of the SMF-COF-SMF structure devices includes the usual process to splice optical fiber. The following steps were realized to manufacture the devices: First, after strip, clean, and cleave both first ends of capillary and single-mode fiber, both fibers are spliced by using a standard fiber optic fusion splicing machine. Then, to cut the capillary fiber at the exact point that corresponds to the desired length of the manufactured device, the spliced point of the first step is placed at the cleaving knife of the optical fiber cleaver, after that, through a linear translation stage, the spliced point is linearly displaced the desired length for the capillary fiber to have. This way, the capillary fiber of the spliced fiber is set in the exact place of the optical fiber cleaver to be cut it at its corresponding length. Next, the capillary fiber is cleaved and spliced to another stripped, cleaned, and cleaved SMF end.

As the fabrication of the device involves the use of a standard fusion splicing machine to splice SMF to capillary fiber, and its manufacture includes the usual process to splice optical fiber. In this work, to obtain as low as possible undeformed splices, some splicing tests between capillary fiber and SMF were realized to get optimal splicing parameters, such as arc power, exposure time, z push, and initial fiber position, which were found to be not significantly different from those of the splicing programs to splice SMF to SMF. Once the optimal splicing parameters were obtained, the fabrication of

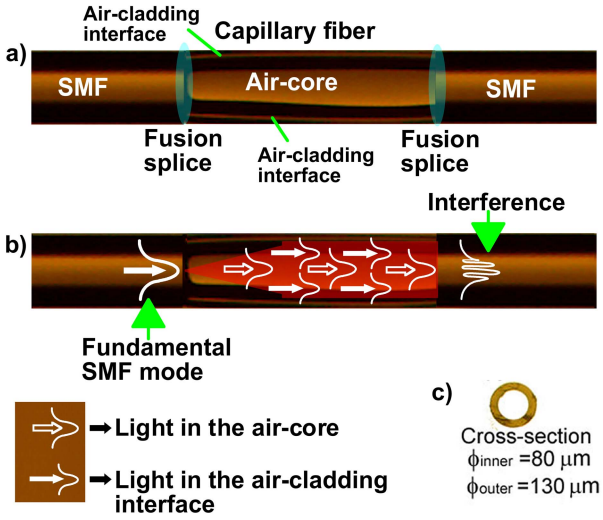

Fig. 1. a) Microscope image of a pressure sensor device with ∼1 *mm* long capillary fiber, b) light behavior through the sensor structure, and c) cross-section microscopic image of the capillary fiber.

the pressure sensors was carried out. In the case of mass production of devices, a problem that could arise, to guarantee the same performance of devices with equal capillary fiber length, is how to ensure the fabrication repeatability of many sensors with the same dimensions and geometry. However, this issue can be resolved by the use of designed and standardized fabrication processes with automatized systems in which cuts and splices of fiber are realized carefully with the use of cameras and controlled micro-metric stages, also the utilization of program splices with optimal conditions in a glass processor system used as a fiber splicer, and all the fabrication process realized in a clean room with stable environmental conditions, such as temperature and humidity.

A microscope image of a device structure with a capillary fiber of ∼1 mm long is depicted in Fig. 1a). Also, in Fig. 1 are the light behavior through the structure (Fig. 1b)) and the cross-section of the capillary fiber (Fig. 1c)). The capillary fiber was home-made fabricated with low-quality silica glass (F300) with an inner and outer diameter of 80 and 130 μm, respectively.

The divergence, after a given propagation distance, of the beam which comes out of the SMF to the capillary fiber, can be evaluated by the following simple formula for a beam radius w [27]:

$$w(d) = w_0 \sqrt{1 + \left(\frac{d\lambda}{\pi n_{air} w_0^2} \right)^2} \tag{1}$$

where w_0 is the beam radius at the fiber end, d is the distance from the fiber end, $n_{air} = 1$, and λ is the wavelength light. Assuming a fiber with a core radius of 4.1 μm, with 0.14 of numerical aperture (NA), and a distance d of 1 mm, we obtain a beam radius of $\sim$ 107 μm. As the inner diameter of the capillary fiber is 80 μm, the beam radius of 107 μm means that the beam interacts not only with the air-core of the capillary fiber but also with the capillary wall. This interaction forces the light to travel through two optical paths: one in

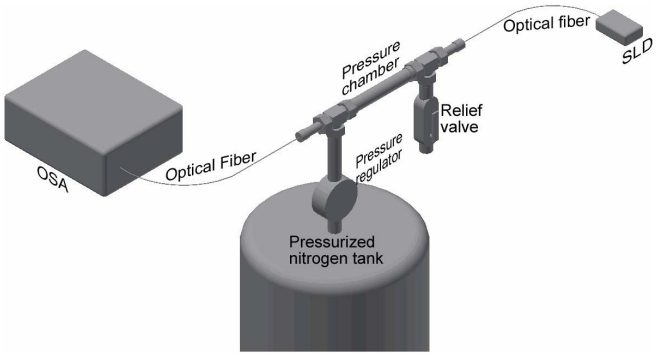

Fig. 2. Experimental setup for measuring pressure employing the capillary optical fiber device.

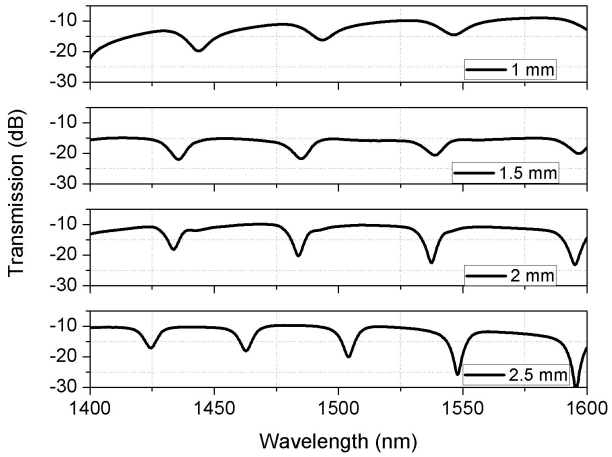

Fig. 3. Transmission spectra for devices with 1, 1.5, 2, and 2.5 *mm* long segments of capillary fiber.

the air-wall boundary (air-cladding interface formed with the air-core of the capillary and the capillary wall), and the other path directly in the air-core (see Fig. 1a) and Fig. 1b)). This way, the structure of the device presented in this work forms the two arms of an interferometer, and therefore the operation principle of the device is the type of a modal Mach-Zehnder interferometer, where the light comes out of the first SMF face, it diverges until arriving the capillary fiberglass, then, the light is guided through the two optical paths in the capillary fiber to generate a phase difference which is given by [32]:

$$\Delta\phi = \frac{2\pi}{\lambda}(n_{eff}^{air-clad} - n_{air})L \tag{2}$$

where λ is the operating wavelength, L is the capillary fiber length, $n_{eff}^{air-clad}$ and n_{air} are the effective refractive indexes of the light which is propagated through the air-cladding interface and air-core of the capillary fiber, respectively. These two divided light are then coupled into the core of the second SMF, producing an interference pattern due to the phase difference between them.

In Fig. 2, the experimental setup for the characterization of the pressure sensor is illustrated, it consists of a superluminescent diode (SLD) as the light source, and an optical spectrum analyzer (OSA) as the detector. The SMF–COF–SMF sensing device was placed inside of a sealed tube (pressure chamber), which was pressurized with nitrogen to apply pressure values from atmospheric pressure to 1000 psi, in steps of 200 psi. The applied pressure was controlled and monitored by a relief valve and a pressure regulator. As the pressure is changed inside the chamber, the capillary fiberglass suffers a stress-induced refractive index anisotropy caused by the compression of the pressure forces. This refractive index change is due to the stress-optic effect or photoelastic effect [33], which induces birefringence variations in the glass material of the capillary fiber. Those alterations in the structure of the capillary fiber cause a direct change of the $n_{eff}^{air-clad}$ from equation 2, altering the phase difference. It is well known that a phase difference change in a fiber optic interferometer causes visibility changes and a wavelength shift of the notches in the interference pattern [20], [34]. In this work, the visibility changes are directly correlated to pressure values. Thus, pressure applied values can be determined from visibility changes in the transmitted spectrum of the proposed sensor.

The induced birefringence in a glass tube, which is caused by pressure forces, at a radial horizontal position R inside the glass wall can be estimated by [31]:

$$B_{glass-tube}(R) = 2(C_2 - C_1)(P_{out} - P_{in})\left(1 - \left(\frac{r_{in}}{r_{out}}\right)^2\right)^{-1}\frac{r_{in}^2}{R^2} \tag{3}$$

where C_1 and C_2 are the elasto–optic coefficients for silica glass ($-0.69X10^{-12}\ Pa^{-1}$ and $-4.19X10^{-12}\ Pa^{-1}$, respectively), P_{in} and P_{out} are the internal and external pressure of the capillary fiber tube, r_{in} and r_{out} are the inner and outer radii of the tube.

III. Experimental Results and Analysis

It is worth to mention that all the experiments presented in this work were repeated at least three times, and the results presented in this section are an average. Also, from the repeated tests, it was found that the sensor behaviors are consistent and have maximum standard deviation values of the order of 4.245×10^{-8}.

The optical transmission spectra for devices with capillary fiber length sections of 1, 1.5, 2, and 2.5 mm long are shown in Fig. 3. It is noted that the fringe contrast or visibility increases as the length of capillary fiber increases. Also, as the length of the capillary fiber increases, the period of the interference fringes decreases. This period behavior is consistent with the free spectral range (FSR), which represents the wavelength difference between two adjacent interference fringes, which is inversely proportional to the capillary fiber length. The FSR is given by the formula [35]:

$$FSR = \lambda_{m-1} - \lambda_m = \frac{\lambda_{m-1}\lambda_m}{L(n_{eff}^{air-clad} - n_{air})} \tag{4}$$

where λ_m and λ_{m-1} are the wavelength of the mth and $(m-1)$th order interference dips and m is an integer. L, $n_{eff}^{air-clad}$, and n_{air} are the same parameters described in equation 2.

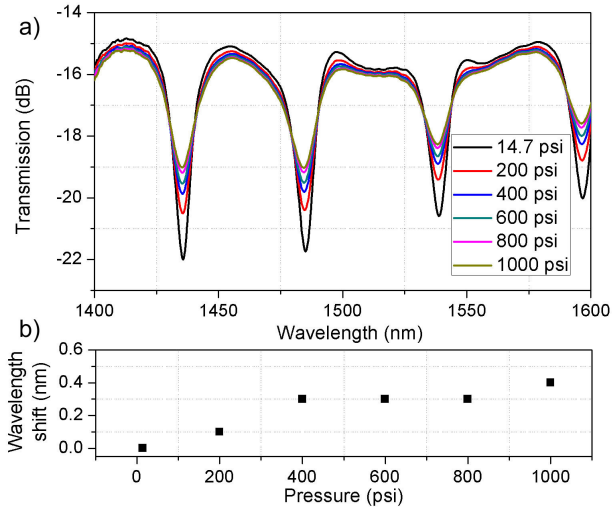

Fig. 4. a) Transmission spectra of a device with a capillary fiber length of 1.5 mm for different pressure values. b) Wavelength shift vs. applied pressure.

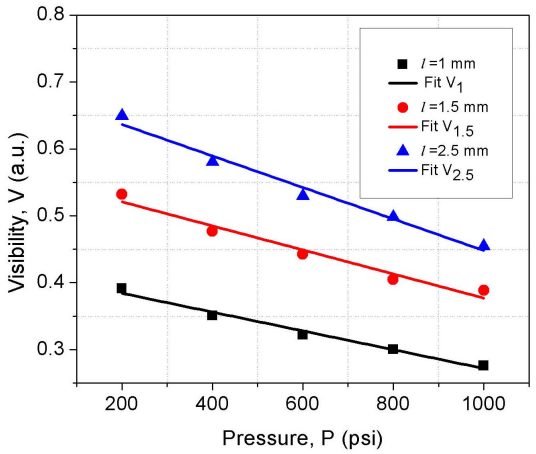

Fig. 5. Experimental and fitting data of the visibility in the transmission spectra for devices with capillary fiber lengths of 1, 1.5, and 2.5 mm, for pressure values ranging from 200 to 1000 psi.

Another effect that occurs when changing the FSR in optical fiber Mach-Zehnder interferometers, by geometrical changes in their structures, is the displacement of the most profound wavelength dip [36]. In this work, it is observed in Fig. 3 that the most profound wavelength dip moves to longer wavelengths as the FSR decreases or the length of capillary fiber augments.

In a variety of optical fiber interferometers, the fringe visibility is employed to determine the quality of their interference patterns, and hence, the quality of any interferometric sensing application [37]. In this work, it was experimentally found that visibility of the interference pattern is affected by pressure changes applied to the device inside the chamber. Fig. 4a) shows the transmission spectra for a fiber device with a capillary fiber length of 1.5 mm from atmospheric pressure to 1000 psi, in steps of 200 psi. According to this figure, it is clear that the fringe visibility decreases as the applied pressure increases. Fig. 4b) shows the wavelength shift caused by the pressure changes, and the maximum wavelength shift was around 0.4 nm over this range of pressures.

The well-known relationship for the fringe visibility (equation 5) was used to evaluate the visibility variations caused by pressure changes in devices with 1, 1.5, and 2.5 mm capillary fiber lengths.

$$V = \frac{I_{up} - I_{low}}{I_{up} + I_{low}} \tag{5}$$

Here I_{low} and I_{up} are the minima of the lower and upper envelopes of the transmission spectra, respectively. The spectral induced visibility changes by pressure on the devices are shown in Fig. 5. The visibility decreases when increasing pressure for all devices. Starting at atmospheric pressure, the visibility values for devices with capillary lengths of 1, 1.5, and 2.5 mm are ∼0.46, ∼0.64, and ∼0.77, respectively. When the pressure inside the chamber is increased to 1000 psi, the visibility values are decreased to ∼0.27, ∼0.39, and ∼0.45 for the capillary lengths of 1, 1.5, and 2.5 mm, respectively. It was found that for pressure values from 200 to 1000 psi, the sensor response to pressure is approximately linear. Fitting the fringe visibility V_l, where l indicates the length of the capillary fiber, of the pressure sensors to linear functions of the applied pressure P, the responses for every sensor are the equations 6, 7, and 8. From those equations, it is observed that the sensitivities of the sensors are approximately -2.356×10^{-4}, -1.798×10^{-4}, and -1.406×10^{-4} $V(a.u.)/psi$ for capillary fiber lengths of 1, 1.5, and 2.5 mm, respectively.

$$V_1 = -2.35627 \times 10^{-4} P + 0.68373 \tag{6}$$

$$V_{1.5} = -1.79766 \times 10^{-4} P + 0.55684 \tag{7}$$

$$V_{2.5} = -1.40614 \times 10^{-4} P + 0.41235 \tag{8}$$

From Fig. 5, it is observed that the dynamic range of pressure measurement is dependent on the length of the capillary fiber. Larger sensor devices are capable of measuring higher pressure values, while smaller devices are limited to measure lower pressure values. As a consequence, the dynamic range of the sensor can be tailored by a proper selection of its capillary fiber length. Also, it can be noted from Fig. 5 that the sensitivity increases as the capillary fiber length increases, which is related to the rise of pressure-sensitive area (capillary fiber) that increases the sensor response.

IV. Response to Temperature of the Capillary Fiber Sensor

An additional characterization to the temperature of the device was performed to find out if temperature induces an effect over the spectrum device, and it could alter the pressure measurements. Several devices were tested under temperature variations by heating them with a hot plate up to 100^0C. Fig. 6 shows the temperature response for a device consisting of 1.5 mm capillary fiber length. It was observed a total wavelength shift of ∼1.6 nm together with a visibility change of ∼0.04 units for the temperature range from room temperature to 100^0C. The calculated sensitivities from linear fits are 0.01871 $nm/^oC$ and $3.1554X10^{-4}$ $V(a.u.)/^oC$ for wavelength shift and visibility changes, respectively.

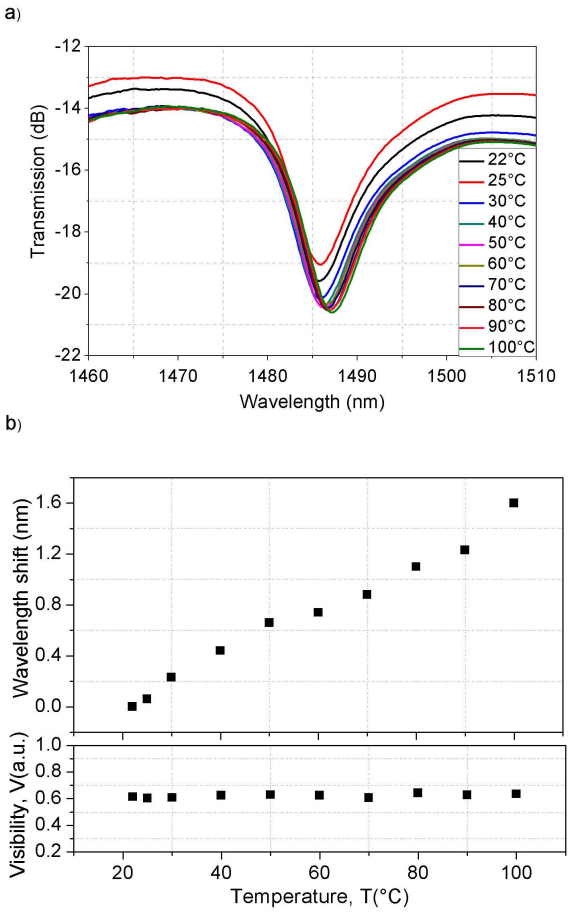

Fig. 6. Temperature response of a sensor with 1.5 *mm* of capillary fiber length; a) spectra for several temperatures ranging from 22 to 100 degrees Celsius, b) wavelength shift and visibility versus temperature (the maximum wavelength shift observed is ∼1.6 *nm*, and the maximum visibility change was ∼0.04 units).

TABLE I
COMPARISON OF THE PROPOSED SENSOR BETWEEN SIMILAR REPORTED PRESSURE SENSORS

References	Working principle	sensitivities	Tested dynamic range
[13]	Air cavity	15 nm/KPa (103.421 nm/psi)	0 to 4 KPa (0 to 0.580151 psi)
[40]	Diaphragm	12.4 nm/KPa (85.49 nm/psi)	1 psi to 7 psi
[41]	Air cavity	$2.8X10^{-4}$ nm/Pa (1.38 nm/psi)	0 to 6.895×10^5 Pa (0 to 100 psi)
[31]	Embedded core in a glass tube	1.04 nm/bar (0.0717 nn/psi)	80 bar (1160.3 psi)
[17]	Special fiber	9.6 nm/MPa (0.066 nm/psi)	0 to 2 MPa (0 to 290.075 psi)
[12]	Air cavity	4.028 nm/MPa (0.0278 nm/psi)	0.2 to 1.2 MPa (29.0075 to 174.045 psi)
Our paper	Capillary (1 mm)	(-0.0002356 $V(a.u.)/psi$)	14.7 to 1000 psi
Our paper	Capillary (1.5 mm)	(-0.0001798 $V(a.u.)/psi$)	14.7 to 1000 psi
[16]	Special fiber	21 pm/MPa (0.00014479 nm/psi)	0 to 45 MPa (0 to 6526.7 psi)
Our paper	Capillary (2.5 mm)	(-0.0001406 $V(a.u.)/psi$)	14.7 to 1000 psi

The transmission spectra for several temperatures ranging from 22 to 100^0C are shown in Fig. 6a). The wavelength shift and visibility for the same range of temperatures are illustrated in Fig. 6b). The capillary glass expansion causes the changes in the wavelength shift and visibility variations, according to the thermal expansion coefficient of the glass ($\sim 5.5X10^{-7}/^0C$) [38]. However, for the pressure sensor operation when the temperature is not constant, those changes can be compensated by the use of a temperature compensation scheme, initial calibrations, or double parameter matrix method. Another fact that is clear to note from Fig. 6 is that for low temperatures (see spectra for 22^oC, 25^oC, 30^oC, and 40^oC in Fig. 6a)) there are higher variations in the spectrum level ($\sim 0.61\ dB$), in contrast with the rest of higher temperatures, where the level of variation is small $\sim 0.1\ dB$. Also, as the temperature increases, the level for each spectrum presented in Fig. 6a) decreases, except for the increase from 22^oC to 25^oC. These facts could be attributed to the release of residual stress stored at the joints between SMF and capillary fiber caused by the fast heat and cooling of the glass [39] in the splicing procedure, this is relaxation of efforts when inducing heat. It is worth to mention that all the tested devices have similar behaviors of these illustrated in this section (visibility variations, level variations, and wavelength shift). Also, as can be noted, the visibility does not change significantly with the temperature, while the wavelength shift increases, which is distinct from the behavior presented in Fig. 4, where both, the transmission and the wavelength shift vary almost equally with the pressure change. A simple explanation of this is that both responses are from different perturbations which alter the sensor in a distinct form, for the pressure alteration over the sensor, the disturbance alters directly to the guided light in the air-cladding interface of the capillary fiber by deformation force via the photo-elastic effect, causing a visibility change and a wavelength shift. On the other hand, for the temperature, the perturbation is generated by the thermal expansion coefficient of the capillary fiber, and the generated disturbance creates a small visibility variation, a wavelength shift, and a level variation caused by thermal relaxation of remaining efforts in the optical fiber splices of the devices formed in the manufacturing process.

V. DISCUSSION ABOUT THE SENSOR VIABILITY

The proposed sensor is compared with remarkable reported FOPSs in table I. The FOPSs are listed in descending order of their pressure sensitivity. Also, in table I, it is included the dynamic range for which the sensors were tested.

From the sensitivity values in table I, it is noted that even though the difference between wavelength shift and visibility interrogation, in orders of magnitude, the sensitivity

of our sensor is not as high as the ones based on air cavity, diaphragms, and embedded core in a glass tube, but it is around the same order of the ones constructed on special fibers. However, this lack of high sensitivity can be an advantaged characteristic regarding the sensor performance. A high sensitivity of the sensor involves huge responses with minimal variations of the parameter to measure, which makes the sensor vulnerable to be also extremely sensitive to external perturbations that may not be related to the perturbation of the measured parameter, what adds alterations that lead to incorrect lectures of the sensor. Also, for this case, if the sensor is working to measure pressures and its sensitivity is ultrahigh, a minimal pressure change or fluctuation will result in no consistent lectures of the sensor. So, high sensitivity sensors are appropriated for controlled environments where only the parameter to measure is varied in a subtle way, such as in a laboratory. On the other hand, a moderate sensitivity sensor is favored to measure in environments with disturbances other than the disturbance to be measured, because that disturbances, accordingly to the moderate sensitivity, may slightly alter the sensor performance, and they may be considered negligible, or they may be easily compensated. Consequently, the moderate sensitivity sensor can be more suitable to support pressure fluctuations without adding inconsistent sensor lectures. In consequence, a sensor with a moderate sensitivity value may become more appropriate to be utilized to measure pressure values in real-world applications, and even to in situ applications.

Also, it is worth to mention some aspects of every FOPS depending on its working principle. Firstly, most of the FOPSs based on air cavities are fabricated with the use of a femtosecond laser, which increases the cost of fabrication. Also, the difficulty of their manufacture is of high level, thus making it difficult for the fabrication repeatability of sensors with identical dimensions and characteristics [12]. A specific case is the one proposed by Ying Wang *et al.* [13], where they use a liquid to act as a transducer, making the sensor complex and limited to specific applications because the sensor performance is affected by the liquid environment conditions. Secondly, the FOPSs based on diaphragms, due to the required equipment and laborious steps for their fabrication, they exhibit delicate, complicated, and expensive fabrication processes, and most of them have a complex construction. Thirdly, the embedded core fiber in a glass tube has complicated and costly fabrication because of the embedded core in the glass tube, and also, it has a complex experimental setup because of the need for free-space-optical alignments, what can make difficult its use in practical applications. And fourthly, the use of special fibers, which sensitivity values are around of the order of our sensor, are also expensive and no very accessible for the use of uncommon costly fibers, and some of them need an additional process, such as, the construction of a micro-channel [17].

Another aspect of being considered is the dynamic range of the sensors. In table I, the dynamic ranges for which every sensor was tested are included. Although all the OFPSs in table I have adequate dynamic ranges for satisfactory pressure sensor measurements. Except for [31], where the adjustment of the dynamic range lies in the change of the sensing fiber size, it is not reported a possible adjustment of the dynamic ranges of the others OFPSs. Also, for [31], the change of the sensing fiber is not an easy task since the manufacture of the sensor is not simple. On the other hand, a simple adjustment of the dynamic range for our sensor can be accomplished by changing the length of the capillary fiber, which can be done just by realizing simple optical fiber splice processes.

Unlike the other OFPSs, the reported sensor in this article shows to have simplicity, easy fabrication, simple experimental setup, cost-effective, easy installation, simple operation, accessibility, and cost-effective construction, which are excellent advantages that exhibit our sensor over the other proposed sensors. Furthermore, our sensor offers a faster, more accessible, and more straightforward approach to measure pressure. Adding the capability of the easy adjustment of its dynamic range, which is a characteristic that most of the FOPSs do not have, our sensor is a good candidate for applications that demand pressure measurements in a simple, practical, fast, and cost-effective way.

Another aspect to consider regarding the proposed devices presented in this work is that they show to have losses between 10 to 15 dB, which can be specially noticed from the normalized spectra of Fig. 3. However, this is a minuscule disadvantage that can be easily compensated with the usage of light sources with power levels upper than these insertion losses, which is not a significant obstacle since most of the conventional light sources have enough power levels that cover with this requirement.

VI. Conclusions

In conclusion, an optical fiber pressure sensor is experimentally demonstrated. The device consists of a capillary optical fiber whose length is only a few millimeters. The device was built using a standard fiber splicer to connect the capillary fiber to standard optical fiber (SMF) and construct an SMF–COF–SMF structure, which acts as a Mach-Zehnder interferometer. Light from the core of the lead-in SMF is launched into the capillary fiber (at the first splice) to travel through two different optical paths (air-core and air-cladding interface in the capillary fiber). Then, when the light from the two paths is coupled to the core of the lead-out SMF at the second splice, interference occurs due to a phase difference generated by the optical path difference between the light of the two different paths. Finally, an interference pattern is collected from the lead-out SMF end. The devices were placed inside of a high-pressure chamber to be pressurized from atmospheric pressure up to 1000 psi. The interference pattern of sensor devices were monitored when applying pressure into the chamber. The applied pressure induces a compression stress distribution forces on the capillary fiberglass, which causes a refractive index change due to the photo-elastic effect. This refractive index change provokes a change in the contrast or visibility of the fringes of the interference pattern and a wavelength shift. The visibility change is directly correlated to the applied pressure by a linear factor in the range from 200 to 1000 psi. Also, as an advantage, the dynamic range of the sensor can be easily tailored through the appropriate

selection of the capillary fiber length. Moreover, in this work, it is presented a practical and straightforward approach to measure pressure by utilizing a device that acts as a transducer by itself, and it is compact, novel, effortless, low cost, and easy to manufacture. Consequently, our pressure sensor is attractive, suitable, feasible, and reliable to monitor the pressure for the well-functioning in industrial processes and industrial operations to avoid injuries and to operate machinery safely. These industrial processes and technical procedures may include hydro-pneumatic systems, compressors, high-pressure boilers, pipes, turbines, and pneumatic systems, which are involved, especially in machinery for manufacturing and production processes.

REFERENCES

[1] F. Urban, J. Kadlec, R. Vlach, and R. Kuchta, "Design of a pressure sensor based on optical fiber BRAGG grating lateral deformation," *Sensors*, vol. 10, no. 12, pp. 11212–11225, 2010.

[2] B. Lee, "Review of the present status of optical fiber sensors," *Opt. Fiber Technol.*, vol. 9, no. 2, pp. 57–79, 2003.

[3] Y.-J. Rao, "Recent progress in fiber-optic extrinsic Fabry–Perot interferometric sensors," *Opt. Fiber Technol.*, vol. 12, pp. 227–237, Jul. 2006.

[4] X. Wang *et al.*, "Verifying an all fused silica miniature optical fiber tip pressure sensor performance with turbine engine field test," *Proc. SPIE*, vol. 5998, Nov. 2005, Art. no. 59980L.

[5] D. Donlagic and E. Cibula, "All-fiber high-sensitivity pressure sensor with SiO_2 diaphragm," *Opt. Lett.*, vol. 30, no. 16, pp. 2071–2073, 2005.

[6] F. Xu *et al.*, "High-sensitivity Fabry–Perot interferometric pressure sensor based on a nanothick silver diaphragm," *Opt. Lett.*, vol. 37, no. 2, pp. 133–135, Jan. 2012.

[7] J. Ma, W. Jin, H. L. Ho, and J. Y. Dai, "High-sensitivity fiber-tip pressure sensor with graphene diaphragm," *Opt. Lett.*, vol. 37, no. 13, pp. 2493–2495, 2012.

[8] C. M. Lawson and V. J. Tekippe, "Fiber-optic diaphragm-curvature pressure transducer," *Opt. Lett.*, vol. 8, no. 5, pp. 286–288, 1983.

[9] T. W. Kao and H. F. Taylor, "High-sensitivity intrinsic fiber-optic Fabry–Pérot pressure sensor," *Opt. Lett.*, vol. 21, no. 8, pp. 615–617, Apr. 1996.

[10] H. Bae and M. Yu, "Miniature Fabry–Pérot pressure sensor created by using UV-molding process with an optical fiber based mold," *Opt. Express*, vol. 20, no. 13, pp. 14573–14583, 2012.

[11] M. Li, M. Wang, and H. Li, "Optical MEMS pressure sensor based on Fabry–Pérot interferometry," *Opt. Express*, vol. 14, no. 4, pp. 1497–1504, 2006.

[12] B. Xu, Y. Liu, D. Wang, D. Jia, and C. Jiang, "Optical fiber Fabry–Pérot interferometer based on an air cavity for gas pressure sensing," *IEEE Photon. J.*, vol. 9, no. 2, Apr. 2017, Art. no. 7102309.

[13] Y. Wang, D. N. Wang, C. Wang, and T. Hu, "Compressible fiber optic micro-Fabry–Pérot cavity with ultra-high pressure sensitivity," *Opt. Express*, vol. 21, no. 12, pp. 14084–14089, 2013.

[14] W. Zhang, F. Li, and Y. Liu, "FBG pressure sensor based on the double shell cylinder with temperature compensation," *Measurement*, vol. 42, no. 3, pp. 408–411, 2009.

[15] H. Sakata and T. Iwazaki, "Sensitivity-variable fiber optic pressure sensors using microbend fiber gratings," *Opt. Commun.*, vol. 282, no. 23, pp. 4532–4536, 2009.

[16] Z. Liu, M.-L. V. Tse, C. Wu, D. Chen, C. Lu, and H.-Y. Tam, "Intermodal coupling of supermodes in a twin-core photonic crystal fiber and its application as a pressure sensor," *Opt. Express*, vol. 20, no. 19, pp. 21749–21757, Sep. 2012.

[17] Z. Li *et al.*, "Highly-sensitive gas pressure sensor using twin-core fiber based in-line Mach–Zehnder interferometer," *Opt. Express*, vol. 23, no. 5, pp. 6673–6678, Mar. 2015.

[18] V. I. Ruiz-Pérez, M. A. Basurto-Pensado, P. LiKamWa, J. J. Sánchez-Mondragón, and D. A. May-Arrioja, "Fiber optic pressure sensor using multimode interference," *J. Phys., Conf. Ser.*, vol. 274, no. 1, 2011, Art. no. 012025.

[19] J. E. Antonio-Lopez, Z. S. Eznaveh, P. LiKamWa, A. Schülzgen, and R. Amezcua-Correa, "Multicore fiber sensor for high-temperature applications up to 1000°C," *Opt. Lett.*, vol. 39, no. 15, pp. 4309–4312, 2014.

[20] G. Salceda-Delgado, A. Van Newkirk, J. E. Antonio-Lopez, A. Martinez-Rios, A. Schülzgen, and R. A. Correa, "Compact fiber-optic curvature sensor based on super-mode interference in a seven-core fiber," *Opt. Lett.*, vol. 40, no. 7, pp. 1468–1471, 2015.

[21] A. Van Newkirk, E. Antonio-Lopez, G. Salceda-Delgado, R. Amezcua-Correa, and A. Schülzgen, "Optimization of multicore fiber for high-temperature sensing," *Opt. Lett.*, vol. 39, no. 16, pp. 4812–4815, 2014.

[22] A. Van Newkirk, J. E. Antonio-Lopez, G. Salceda-Delgado, M. U. Piracha, R. Amezcua-Correa, and A. Schülzgen, "Multicore fiber sensors for simultaneous measurement of force and temperature," *IEEE Photon. Technol. Lett.*, vol. 27, no. 14, pp. 1523–1526, Jul. 15, 2015.

[23] R. Jha, J. Villatoro, G. Badenes, and V. Pruneri, "Refractometry based on a photonic crystal fiber interferometer," *Opt. Lett.*, vol. 34, no. 5, pp. 617–619, Mar. 2009.

[24] R. Gao, Y. Jiang, and Y. Zhao, "Magnetic field sensor based on anti-resonant reflecting guidance in the magnetic gel-coated hollow core fiber," *Opt. Lett.*, vol. 39, no. 21, pp. 6293–6296, Nov. 2014.

[25] J. Sirkis *et al.*, "In-line fiber etalon (ILFE) fiber-optic strain sensors," *J. Lightw. Technol.*, vol. 13, no. 7, pp. 1256–1263, Jul. 1995.

[26] A. Dutt, S. Mahapatra, and S. K. Varshney, "Capillary optical fibers: Design and applications for attaining a large effective mode area," *J. Opt. Soc. Amer. B, Opt. Phys.*, vol. 28, no. 6, pp. 1431–1438, 2011.

[27] S. Jiang, B. Zeng, Y. Liang, and B. Li, "Optical fiber sensor for tensile and compressive strain measurements by white-light Fabry–Pérot interferometry," *Opt. Eng.*, vol. 46, no. 3, 2007, Art. no. 034402.

[28] S.-H. Kim, J.-J. Lee, D.-C. Lee, and I.-B. Kwon, "A study on the development of transmission-type extrinsic Fabry–Pérot interferometric optical fiber sensor," *J. Lightw. Technol.*, vol. 17, no. 10, pp. 1869–1874, Oct. 1999.

[29] C. N. Capsalis, N. K. Uzunoglu, and I. G. Tigelis, "Coupling between two abruptly terminated single-mode optical fibers," *J. Opt. Soc. Amer. B, Opt. Phys.*, vol. 5, no. 8, pp. 1624–1630, 1988.

[30] V. Arya, M. De Vries, K. A. Murphy, A. Wang, and R. O. Claus, "Exact analysis of the extrinsic Fabry–Pérot interferometric optical fiber sensor using kirchhoff's diffraction formalism," *Opt. Fiber Technol.*, vol. 1, no. 4, pp. 380–384, 1995.

[31] J. H. Osório, G. Chesini, V. A. Serrão, M. A. R. Franco, and C. M. B. Cordeiro, "Simplifying the design of microstructured optical fibre pressure sensors," *Sci. Rep.*, vol. 7, no. 1, 2017, Art. no. 2990.

[32] M. Park *et al.*, "Ultracompact intrinsic micro air-cavity fiber Mach–Zehnder interferometer," *IEEE Photon. Technol. Lett.*, vol. 21, no. 15, pp. 1027–1029, Aug. 1, 2009.

[33] A. Barlow and D. Payne, "The stress-optic effect in optical fibers," *IEEE J. Quantum Electron.*, vol. QE-19, no. 5, pp. 834–839, May 1983.

[34] G. Salceda-Delgado *et al.* "Adaptable optical fiber displacement-curvature sensor based on a modal michelson interferometer with a tapered single mode fiber," *Sensors*, vol. 17, no. 6, p. 1259, 2017.

[35] X. Sun *et al.*, "Highly sensitive refractive index fiber inline Mach–Zehnder interferometer fabricated by femtosecond laser micromachining and chemical etching," *Opt. Laser Technol.*, vol. 77, pp. 11–15, Mar. 2016.

[36] G. Salceda-Delgado, A. Martinez-Rios, and D. Monzón-Hernández, "Tailoring Mach–Zehnder comb-filters based on concatenated tapers," *J. Lightw. Technol.*, vol. 31, no. 5, pp. 761–767, Mar. 1, 2013.

[37] D. Monzon-Hernandez, A. Martinez-Rios, I. Torres-Gomez, and G. Salceda-Delgado, "Compact optical fiber curvature sensor based on concatenating two tapers," *Opt. Lett.*, vol. 36, no. 22, pp. 4380–4382, Nov. 2011.

[38] G. Salceda-Delgado, D. Monzon-Hernandez, A. M. Martinez-Rios, G. A. Cardenas-Sevilla, and J. Villatoro, "Optical microfiber mode interferometer for temperature-independent refractometric sensing," *Opt. Lett.*, vol. 37, no. 11, pp. 1974–1976, 2012.

[39] A. Yi, B. Tao, F. Klocke, O. Dambon, and F. Wang, "Residual stresses in glass after molding and its influence on optical properties," *Procedia Eng.*, vol. 19, no. 63, pp. 402–406, 2011.

[40] X. Guo, J. Zhou, C. Du, and X. Wang, "Highly sensitive miniature all-silica fiber tip Fabry–Perot pressure sensor," *IEEE Photon. Technol. Lett.*, vol. 31, no. 9, pp. 689–692, May 1, 2019.

[41] Y. Zhang, L. Yuan, X. Lan, A. Kaur, J. Huang, and H. Xiao, "High-temperature fiber-optic Fabry–Perot interferometric pressure sensor fabricated by femtosecond laser," *Opt. Lett.*, vol. 38, pp. 4609–4612, Nov. 2013.

Guillermo Salceda-Delgado was born in Leon, Guanajuato, Mexico, in 1984. He received the B.S. degree in electromechanics from the Instituto Tecnologico de Leon, Mexico, in 2009, and the M.S. and the Ph.D. degrees in ciencias (optica) from the Centro de Investigaciones en Optica (CIO) in 2011 and 2015, respectively.

From 2013 to 2015, he realized a research internship with the College of Optics and Photonics (CREOL), University of Central Florida (UCF), Orlando, Florida, USA, where he was working on the use and fabrication of special fibers, such as multicore and photonic crystal fibers. Since 2015, he has been a Research Professor with the Universidad Autónoma de Nuevo León (UANL), Cd. Universitaria, San Nicolás de los Garza, Nuevo Leon, Mexico. He has a chapter book publication and a total of 44 journal publications and presentations from his research in optical fibers sensor devices and optical fiber lasers with 493 citations at the moment. He has also been in charge of the realization of one project sponsored by the Secretary of Public Education (SEP) under the El Programa de Mejoramiento del Profesorado (PROMEP) and two internal projects in the UANL under the Programa de Apoyo a la Investigacion Cientifica y Tecnologica (PAICYT). He is a member of the Sistema Nacional de Investigadores (SNI), Mexico, belonging to level one. His research interests include the design, fabrication, and use of optical fiber sensor devices and optical fiber lasers.

Amy Van Newkirk received the bachelor's degree in applied physics from the Grove City College, Grove City, PA, USA, and the Ph.D. degree from CREOL, The College of Optics and Photonics, University of Central Florida, under Dr. A. Schülzgen.

She has expertise in specialty optical fiber research, having completed her Ph.D. thesis on specialty fibers for lasers and sensing applications. In her research at CREOL, she investigated a variety of specialty optical fibers in theory and experiment, including multicore fibers for extreme environment sensing and hollow-core fibers for mid-infrared and high-power applications. She joined the Penn State Applied Research Lab, Electro-Optics Center, August 2016, as a Postdoctoral Scholar, where she became an Assistant Research Professor in 2017. Her current work is focused on anti-resonant hollow-core fibers for defense applications, such as precision navigation and tracking and high-power laser delivery. She has a total of 33 journal publications and presentations from her research in specialty optical fibers. She was a recipient of the Air Force Office of Scientific Research Young Investigator Program, which supports her research in hollow-core fibers for high power and MWIR delivery.

Jose Enrique Antonio-Lopez received the Ph.D. degree from the Instituto Nacional de Astrofísica, Óptica y Electrónica (INAOE), San Andres Cholula, Mexico, in 2012, with the work design and fabrication of photonic devices based on multimode interference. He is a Research Scientist with the College of Optics and Photonics (CREOL), University of Central Florida (UCF), Orlando, FL, USA. His research interests include design, fabrication, and use of special fibers. He has a total of 226 journal publications and presentations from his research with 2648 citations, at the moment.

Alejandro Martinez-Rios received the bachelor's degree in electro-mechanical engineering and the Ph.D. degree in optical sciences from the Centro de Investigaciones en Optica, Leon, Guanajuato, Mexico, in 1994 and 2000, respectively. In 2010, he was a Visiting Scholar with the University of California at Merced. He is currently a Principal Researcher with the Centro de Investigaciones en Optica, where he is working on optical fiber lasers and devices. He has a total of 161 journal publications and presentations from his research, with 1112 citations at the moment. He is a level three member of the Sistema Nacional de Investigadores (SNI), Mexico.

Axel Schülzgen received the Ph.D. degree in physics from the Humboldt-University of Berlin, Germany. Since 2009, he has been a Professor of Optics with the College of Optics and Photonics (CREOL), University of Central Florida (UCF), Orlando, FL, USA. He holds an Adjunct Research Professor position at the College of Optical Sciences, University of Arizona. His research interests include optical fiber devices, components, materials, and structures with applications in fiber laser systems, fiber optic sensing, and optical communications. He is a Fellow of the Optical Society of America and a member of the International Society for Optics and Photonics SPIE and the German Physical Society. He has a total of 283 journal publications and presentations from his research with 4295 citations at the moment.

Rodrigo Amezcua-Correa received the Ph.D. degree from the Opto-electronics Research Centre (ORC), University of Southampton with a focus on development of photonic crystal fibers. He joined the College of Optics and Photonics (CREOL), University of Central Florida (UCF), Orlando, FL, USA, and the Townes Laser Institute as an Assistant Research Professor, in February 2011. After completing his Ph.D. research, he was employed as a Postdoctoral Researcher with Prof. J. Knight at the University of Bath, U.K. At the University of Bath, he has developed novel photonic crystal fiber fabrication methods that lead to fibers with significantly improved optical properties. He has extensive experience in the design and fabrication of photonic crystal fibers for several applications, including fiber lasers, supercontinuum generation, nonlinear microscopy, and sensing. Before joining CREOL, he worked at Powerlase Photonics, fabricating high-power diode-pumped solid-state lasers. He has a total of 293 journal publications and presentations from his research with 2903 citations at the moment.